Mapping the electronic structure of polypyrrole with image-based electrochemical scanning tunnelling spectroscopy

Roger Gonçalves[1,2], Robert S. Paiva[1], Andrés M. R. Ramírez[2,3, †], Jonathan A. Mwanda[2, §]

Ernesto C. Pereira[1] and Angel Cuesta[2.*]

[1] *Department of Chemistry, Universidade Federal de São Carlos, Mail Box 676, CEP 13565-905, São Carlos – SP, Brazil*

[2] *Department of Chemistry, School of Natural and Computing Sciences, University of Aberdeen, Aberdeen AB24 3UE, UK*

[3] *Pontificia Universidad Católica de Chile, Laboratorio de Electroquímica de Polímeros (LEP), Av. Vicuña Mackenna 4860, 7820436-Macul, Santiago, Chile*

**Corresponding author:* angel.cuestaciscar@abdn.ac.uk

[†]Current address: *Laboratorio de Electroquímica y Materiales Aplicados, Centro de Nanotecnología Aplicada, Facultad de Ciencias, Universidad Mayor, Av. Alemania 0281, 4801043-Temuco, Chile*

[§]Current address: *Gulf Organization for Research and Development, Doha, Qatar*

Abstract: Conducting polymers are versatile semiconductors whose applications cover a wide range of devices. Their versatility is due, in addition to other factors, to properties that can be easily modulated according to the intended application. It is therefore important to study and map the electronic structure of these materials to allow for a better correlation between structure and properties. Electrochemical scanning tunnelling spectroscopy (EC-STS) can be a powerful tool to characterize the electronic structure of the semiconductor electrolyte interface. In this work we have used image-based EC-STS (IB-EC-STS) to describe quantitatively the band structure of an electrochemically deposited polypyrrole (PPy) film. IB-EC-STS located the band edge of the polymer's valence band (VB) at 0.95 V vs. RHE (-5.33 eV in the absolute potential scale) and the intragap polaron states formed when the polymer is oxidised (doped) at 0.46 V vs. RHE (-4.84 eV in the absolute potential scale). The IB-EC-STS data were cross checked with electrochemical impedance spectroscopy (EIS) and Mott-Schottky analysis of the interfacial capacitance. The DOS spectrum obtained from EIS data is consistent with the STS-deduced location of the VB and the polarons.

Keywords: polypyrrole, electronic structure, electrochemical scanning tunnelling microscopy, impedance spectroscopy.

1. INTRODUCTION

Understanding the electronic structure of conducting polymers (CPs) is necessary for a detailed understanding of the behaviour of these materials, whose mechanism of electronic conduction is different from that characteristic of inorganic semiconductors. It is therefore important to acquire the experimental information required to build a complete model of their band structure, which governs their properties.[1,2]

Due to the size of CP molecules, atomic orbitals in the polymer chains combine to give rise to bands that extend throughout the entire macromolecule.[3] As in the case of inorganic semiconductors, the conductivity of the undoped material is associated to either free electrons in the conduction band (CB) or free holes in the valence band (VB) generated either by photo-excitation or (if the band gap is sufficiently small compared with kT) by thermal excitation of electrons from the VB into the CB. In the case of inorganic semiconductors, the conductivity can be increased by injecting electrons or holes in either the CB or the VB through n or p doping, respectively, which typically results in the creation of an associated point defect in the material. On the other hand, doping of CPs is due to oxidation or reduction processes in the polymer, and does not result in the injection of electrons or holes in the CB or the VB, respectively, but in the formation of solitons, polarons and, at high doping levels, bipolarons, localised within the energy gap.[4,5] In the particular case of p-doping a CP through oxidation, a radical cation (hole-polaron, spin 1/2) is created upon removal of an electron from the polymeric chain,[5] which could be understood as a rearrangement of π electrons that locally polarizes the polymer chain. In chemical terms, a polaron consists of a radical ion with unitary charge and a well-defined energy within the gap that can be detected, *e. g.*, via optical spectroscopy[6] (please note, however, that optical spectroscopy will provide the energy difference between the intragap level and the band edge, but never the exact location of the intragap level in a well-defined energy scale, unless the location of the band edge itself is also known). If a second electron is removed from the polymer chain, two situations can occur: (i) another hole-polaron state is created, or (ii) if the polarons are close enough (*i. e.*, at high doping levels[5,7]) they collapse in a single, doubly charged

defect, called bipolaron. (spin 0).[8–10] In summary, like inorganic semiconductors, CPs can be doped in order to control their conductivity.[11] However, the charge carriers are not electrons or holes inside the CB and VB, respectively, but polarons and bipolarons located within the bandgap.[12]

Polypyrrole (PPy) is one of the most studied CPs because of its low oxidation potential, the water solubility of the monomer and its low cost.[13] These unique properties make it compatible with devices working in aqueous media, in applications like drug delivery, biosensors, artificial muscles and optoelectronic devices.[14] PPy was the first CP to be characterized by its optoelectronic properties, which can be altered by doping/de-doping.[15]

Scanning Tunnelling Microscopy (STM) is a powerful technique based on the quantum tunnelling effect that allows obtaining images of surfaces with atomic resolution.[16] When a sharp metallic tip is placed very close to a sample surface and a small bias voltage is applied, a tunnelling current flows through the gap between them. This tunnelling current can also flow through a liquid electrolyte, and it is measurable if the tip is properly isolated to decrease the magnitude of any faradaic currents below the level of the target tunnelling current, allowing to obtain images with atomic resolution of electrode surfaces.[17,18] The tunnelling current also depends strongly on the density of states, and tunnelling current *vs.* bias plots obtained during a fast scan (typically in the V s^{-1} region) of the tip-sample bias (*i.e.*, scanning tunnelling spectroscopy, STS) have been used to elucidate the band structure of conducting polymers in ultra-high vacuum (UHV).[19] A problem with this approach, however, is that the energy levels obtained by UHV-based STS cannot be related to any useful energy scale, like the reversible hydrogen electrode (RHE) or the absolute potential scale. This could be solved by doing STS at the electrode-electrolyte interface (electrochemical STS, EC-STS), where the potential of both tip and sample can be referred to a common reference electrode, but this is very challenging, because, at the high scan rates needed to scan the tip potential, faradaic and capacitive currents (which scale with the square root of and linearly with, respectively, the scan rate) easily obscure the tunnelling current. A way around this problem is to use imaged-based EC-STS (IB-EC-STS), in which the tip potential *versus* a suitable reference electrode is scanned during imaging in

either positive or negative direction until the STM image disappears, which must coincide with the moment at which a band edge is crossed and the Fermi level of the tip falls within the sample's band gap (where neither tunnelling from the tip to the full VB nor from the empty CB to the tip is possible). This approach was used by Sanz and co-workers[20] to elucidate the band structure of the passive film on an iron electrode, and that work remains, to the best of our knowledge, the only example of IB-EC-STS

In this work, IB-EC-TS, and energy-resolved electrochemical impedance spectroscopy (EIS) where combined to map the electronic structure of a PPy film and to obtain a quantitative description of its electronic structure.

2. EXPERIMENTAL SECTION

2.1. Solutions and reactants. PPy was synthesised from pyrrole (Sigma-Aldrich) without further purification. For both electrosynthesis and electrochemical aqueous characterization, the electrolyte used was 0.1 mol L-1 HClO4 (70%, Sigma-Aldrich) prepared using ultra-pure Milli-Q water (resistivity of 18.0 MΩ cm).

2.2. Cyclic voltammetry and electrochemical impedance spectroscopy. Cyclic voltammetry and electrochemical impedance spectroscopy were performed using a conventional three-electrode configuration. The working electrode was either a Pt(111) single-crystal (prepared as described in Section 2.3) or a polycrystalline platinum electrode covered with PPy, with the substrate having no effect on the behaviour of the PPy film, and a Pt wire was used as counter electrode. A reversible hydrogen electrode (RHE) was used as reference. PPy films were synthetized electrochemically via cyclic voltammetry in a conventional three-electrode cell containing 0.1 mol L^{-1} HClO$_4$ + 0.1 mol L^{-1} pyrrole. The working electrode was cycled 10 times at 50 mV s^{-1} in the potential range between 0.0 V and 1.0 V vs. RHE. After the PPy growth, the substrate covered with the polymer film was rinsed with water and placed in an electrochemical cell containing pyrrole-free 0.1 mol L^{-1} HClO$_4$ for the measurements. Cyclic voltammetry was carried out between 0.0 V and 1.0 V at a scan rate of 0.05 V s^{-1}, starting at 0.1 V in the positive direction to ensure that the PPy film was initially in the reduced (de-doped) state. The interfacial capacitance and the charge transfer resistance were determined at selected potentials by fitting the corresponding electrochemical impedance (EI) spectra to a transmission line model (see Supporting Information). EI spectra were obtained by scanning the frequency between 10 kHz and to 0.1 Hz, with an ac perturbation of 0.01 V.

2.3. ***STM characterization.*** STM cells used were kept for at least 24 hours in piranha solution (H_2SO_4 / H_2O_2, 9:1) prior to use. They were then rinsed several times with ultra-pure water and boiled in ultra-pure water for half an hour, repeating the rinsing and boiling procedure at least 4 times. The Pt(111) electrode used for STM measurements was annealed in the flame of a Bunsen burner and then allowed to cool down to room temperature inside a flask containing a N_2 + H_2 atmosphere.

Pt-Ir (80:20) tips were prepared by an electrochemical etching procedure,[21–23] a detailed description of which can be found in the Supplementary Information. Once etched, the tips were insulated using an electrophoretic paint in order to lower capacitive and faradaic currents down to a few pA or, at most, tens of pA. Details of the insulating procedure can be found in the Supplementary Information.

STM images were recorded using a PicoLE Molecular Imaging with a PicoScan 2100 controller. Pt wires were used as counter and *quasi* reference electrodes.

3. RESULTS AND DISCUSSION

3.1. ***Electrochemical characterization.*** Figure 1a shows the cyclic voltammograms recorded during the growth of a PPy film on a Pt(111) electrode in a perchloric acid solution containing pyrrole. During growth, the current in the double-layer region increases linearly with increasing number of cycles (Fig. 1a, inset), as expected. After growth, the voltammetric profile of the PPy film in a pyrrole-free perchloric acid solution agrees with those described in previous work for PPy in acidic media (Figure 1b).[24–26] The cyclic voltammogram is characterised by an oxidation process that starts around 0.12 V and peaks around 0.49 V, corresponding to the p-doping of the polymer.
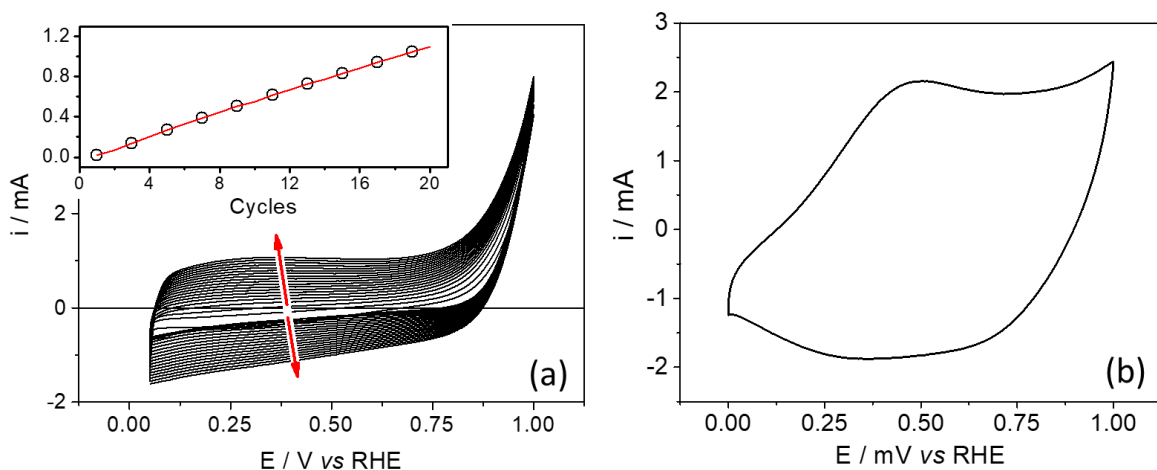
Figure 1. (a) Cyclic voltammograms recorded during the growth of polypyrrole from 0.1 mol L^{-1} HClO$_4$ + 0.1 mol L^{-1} pyrrole solutions on a Pt(111) electrode. The inset shows the linear increase of the current at 0.04 V with increasing number of cycles; **(b)** cyclic voltammetry of PPy on Pt(111) in pyrrole-free 0.1 M HClO$_4$ mol L^{-1}. Scan rate: 0.05 V s^{-1}.

Electrochemical impedance spectroscopy was used to obtain information about the electrochemical and electronic properties of the PPy film. The impedance results were fitted using a transmission line model[24,27–31], which is presented in the Supplementary Information (Part 2). A plot of the inverse of the squared capacitance, as obtained from the impedance measurements, can be used to determine the apparent charge-carrier density and the apparent flat-band potential by fitting the data to the Mott-Schottky equation:

$$\frac{1}{C^2} = \frac{2}{\varepsilon_r \varepsilon_0 e N_h}\left(E_{fb} - E + \frac{k_B T}{e}\right)$$ Equation 1

Where ε_r is the material's dielectric constant, ε_0 is the vacuum permittivity, e is the elementary charge, N_h, is the density of majority charge carriers (in the PPy case, polaron and, at high doping levels, bipolaron holes), E_{fb} is the flat-band potential, E is the applied potential, k_B is the Boltzmann constant and T is the temperature in Kelvin. Figure 2a shows such a plot and fit, from where an apparent flat-band potential of 0.11 V and an apparent hole polaron density of 3.31 sx 10^{19} cm^{-3} is obtained. We will discuss these values later, in the light of the information obtained from the impedance-derived distribution of density of states (DOS) and the IB-EC-STS data.

The potential dependent charge transfer resistance (R_{ct}), as obtained from EIS, can be used to calculate the DOS spectrum using the Gmucová-Nádaždy equation[32,33]:

$$\left(E_{fb,redox} = eU\right) = \frac{1}{ek_{et}[A]SR_{ct}} \qquad \text{Equation 2}$$

Where e is the elementary charge, k_{et}, is the charge-transfer constant in cm^4 s^{-1}, [A] is the concentration in the electrolyte of redox (donor/acceptor) pairs in cm^{-3}, S is the electrode area in cm^2 and R_{ct} is the charge-transfer resistance in Ω. Figure 2b shows the DOS spectrum of our PPy films, from which a location of the VB edge at 0.95 V can be estimated. This value will be compared below with that obtained from IB-EC-STS.
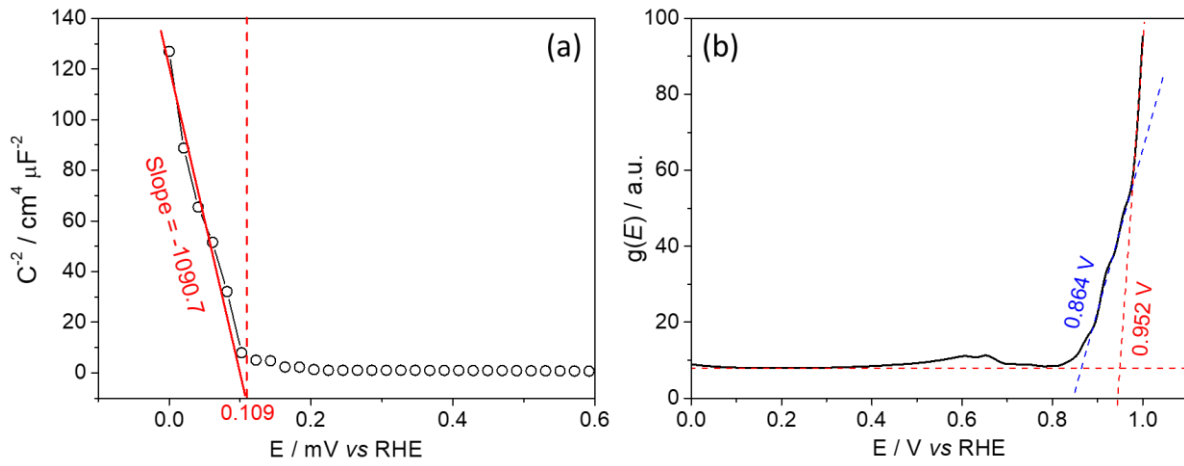
Figure 2. Mott-Schottky plot **(a)** and density of states (DOS) spectrum **(b)** of a thin film of polypyrrole grown on polycrystalline Pt after 20 voltammetric cycles.

3.2. ***Image-based electrochemical scanning tunnelling spectroscopy.*** Fig. 3 shows an STM image recorded at a sample potential $E_{Sample} = 0.25$ V, at which, according to the cyclic voltammogram in Fig. 1(b), the PPy film must have been slightly oxidised (i.e., some hole polarons must have been created), and an initial tip potential $E_{Tip} = 0.55$ V. Under these conditions, imaging should be impossible, because electrons should tunnel from the sample (more negative potential, equivalently, higher E_F) to the tip (more positive potential, equivalently, lower E_F) but, according to the DOS spectrum in Fig. 2b, the E_F of the tip lies exactly within the PPy's band gap and there are no occupied states from which this could happen.
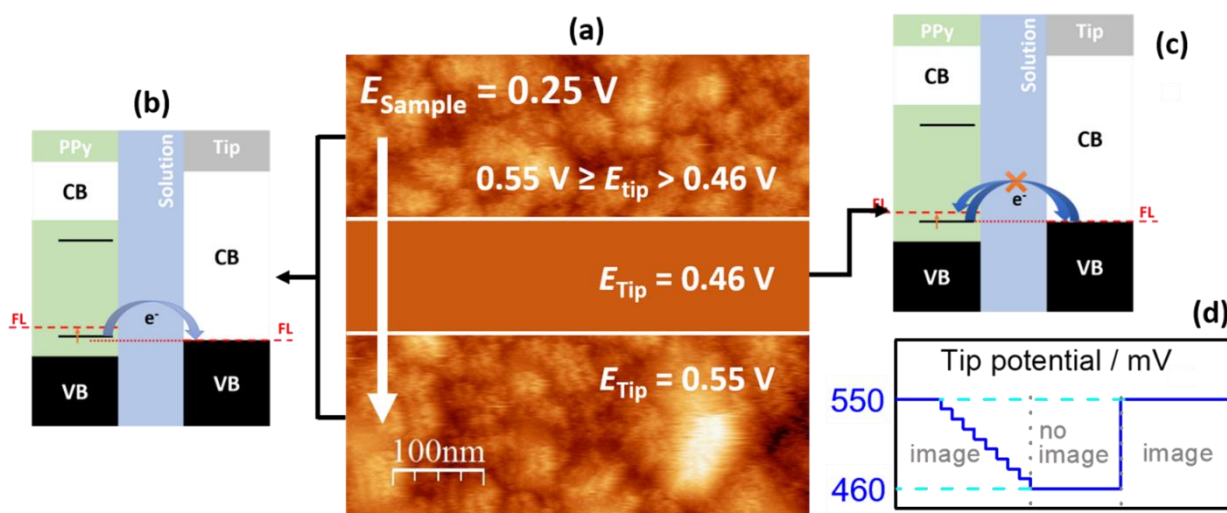
Figure 3. (a) STM image (500 x 500 nm^2) of a PPy film electrochemically grown on a Pt(111) electrode in 0.1 mol L^{-1} HClO$_4$ at $E_{sample} = 0.25$ V. The scan direction is from top to bottom, as indicated by the white arrow. Initially, $E_{tip} = 0.55$ V. E_{tip} was then progressively made more negative in 0.01 V steps. The central region of the image was recorded at $E_{tip} = 0.46$ V, and then E_{tip} was stepped back to the initial value of 0.55 V before recording the bottom part of the image; **(b)** Schematic representation of the location of the different energy levels when $E_{tip} = 0.55$ V, with electrons tunnelling from the intra-gap, half-filled, polaron hole state into the tip's Fermi level. The effect of band bending has been omitted for the sake of clarity and simplicity; **(c)** Schematic representation of the location of the different energy levels when $E_{tip} \leq 0.46$ V. Tunnelling is not possible either from the tip to the sample due to the positive tip bias, or from the sample to the tip, because there are no filled or partially filled electronic states above the tip's Fermi level. The effect of band bending has been omitted for the sake of clarity and simplicity; **(d)** Scheme illustrating the potential programme applied to the tip. $I_T = 2$ nA.

A clear image can however be obtained (Fig. 3a), which can only be explained if a half-filled polaron level is located at an energy higher than the tip's E_F. In order to test this hypothesis, the tip potential was slowly scanned in the negative direction, which results in the image disappearing at 0.46 V (Fig. 3a). The image reappears if the tip potential is then stepped back to 0.55 V, as shown in the lower part of the image (Fig. 3a). This allows us to locate the position of the hole polaron at 0.46 V vs. RHE, which is in good agreement with the small DOS between 0.4 and 0.7 V in the DOS spectrum in Fig. 2b. The behaviour observed in Fig. 3 can be explained as follows: when $E_{tip} \leq 0.46$ V but more positive than the sample potential (0.25 V), the flow of electrons from the sample to the tip (as dictated by the positive tip bias) is not possible because the VB edge is lower in energy than the tip's Fermi level, and the electronic states in the CB are all empty at room temperature (Fig. 3c).

On the contrary, when $E_{tip} > 0.46$ V, the tip's energy level lies at a lower level than the half-filled polaron hole, which allows electrons to tunnel from the latter into the tip and a STM image to be established (Fig. 3b).

The experiment shown in Fig. 4 confirms that imaging in the top and bottom sections of Fig. 3a was due to tunnelling from intra-gap, half-filled polaron states. As in Fig. 3, E_{Tip} and E_{Sample} were initially set at 0.55 and 0.25 V, respectively. A clear image was obtained under these conditions, reproducing the results in Fig. 3a. Instead of changing E_{Tip}, as in Fig. 3, in this experiment E_{Tip} was kept constant and E_{Sample} was stepped to 0.10 V after having scanned approximately ¼ of the image area (Fig. 4a). According to the cyclic voltammogram in Fig. 1b, at 0.1 V the oxidised polymer units should be reduced, in other words, this potential step should result in the de-doping of PPy and the disappearance of the half-filled polaron states. As expected, the image vanishes after the potential step (Fig. 4a), confirming that imaging was due to tunnelling from the hole polaron states (see Figs. 4b and c). E_{Tip} was then slowly made more positive until the image reappeared at $E_{tip} = 0.95$ V (Fig. 4a). This must correspond to the potential at which the Fermi level of the tip crosses the VB edge, allowing the tip to receive electrons from the VB (Figure 4d). This is in excellent agreement with the location of the VB edge as obtained from the EIS-derived DOS spectrum.
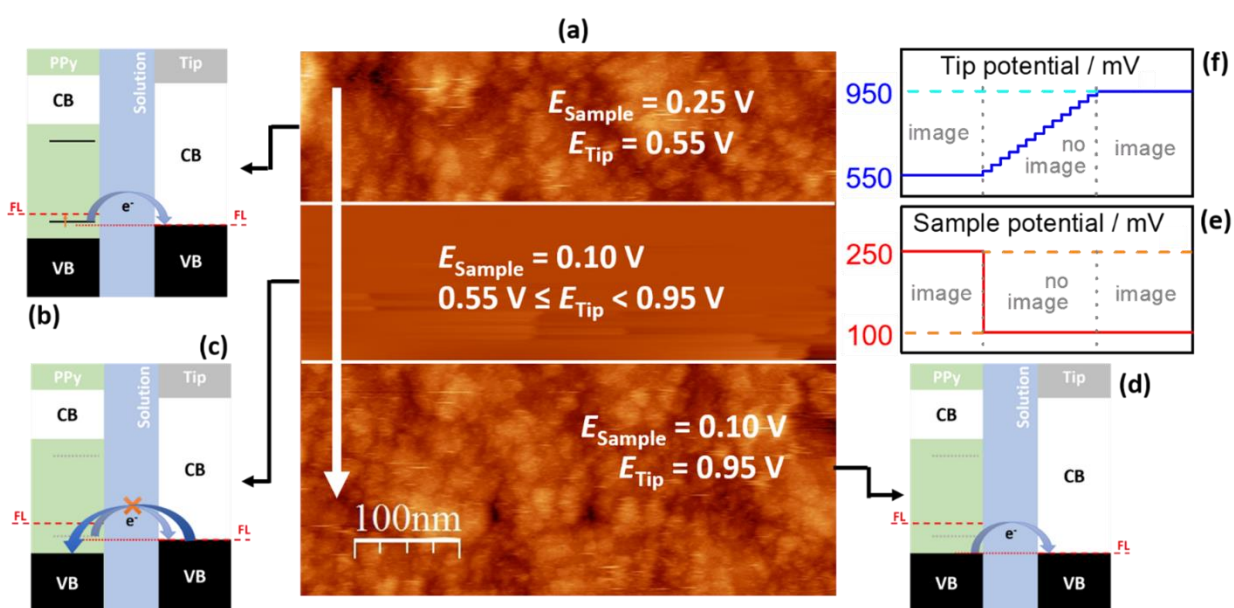

Figure 4. (a) STM image (500 x 500 nm^2) of a PPy film electrochemically grown on a Pt(111) electrode in 0.1 mol L^{-1} HClO$_4$ at initial $E_{sample} = 0.25$ V and $E_{tip} = 0.55$ V. The scan direction is from top to bottom, as

indicated by the white arrow. E_{sample} was stepped to 0.10 V approximately one quarter down the image. The central region of the image was recorded at $E_{sample} = 0.10$ V while E_{tip} was increased from 0.55 to 0.95 V in 0.01 V steps. The bottom section of the image was recorded at $E_{sample} = 0.10$ V and $E_{tip} = 0.95$ V; **(b)** Schematic representation of the location of the different energy levels when $E_{tip} = 0.55$ V and $E_{sample} = 0.25$ V, with electrons tunnelling from the intra-gap, half-filled, polaron hole state into the tip's Fermi level. The effect of band bending has been omitted for the sake of clarity and simplicity; **(c)** Schematic representation of the location of the different energy levels when $E_{sample} = 0.10$ V and 0.55 V $\leq E_{tip} < 0.95$ V. Tunnelling is not possible either from the tip to the sample due to the positive tip bias or from the sample to the tip, because there are no filled or partially filled electronic states above the tip's Fermi level. The effect of band bending has been omitted for the sake of clarity and simplicity; **(d)** Schematic representation of the location of the different energy levels when $E_{sample} = 0.10$ V and $E_{tip} = 0.95$ V. Tunnelling is now possible from PPy's VB into the tip's Fermi level; **(e) and (f)** Schemes illustrating the potential programmes applied to sample and tip, respectively. $I_T = 2$ nA.

Because hole polaron levels are half filled, tunnelling from the tip to these levels must be possible under negative tip bias. This is confirmed by the results in Fig. 5. In this case, E_{Sample} was set at 0.25 V and E_{Tip} was initially set at 0.49 V. As we have seen above, polaron states have already been created at this E_{Sample}, and tunnelling from these to the tip results in a clear STM image (Figs. 5a and b). E_{Tip} was then slowly scanned in the negative direction in 0.10 V steps, until the polaron level is crossed at 0.43 V (please note that a Pt wire was used as quasi-reference in these spectra, which accounts for the small difference in the location of the polaron level in Figs. 3 and 5), at which the image disappears for the reasons explained above (Figs. 5a and c). However, when the E_{Tip} reaches a value of 0.29 V and the tip crosses the sample's Fermi level, the STM image is recovered because now electrons can tunnel from the tip to the half-filled polaron level (Figs. 5a and d).
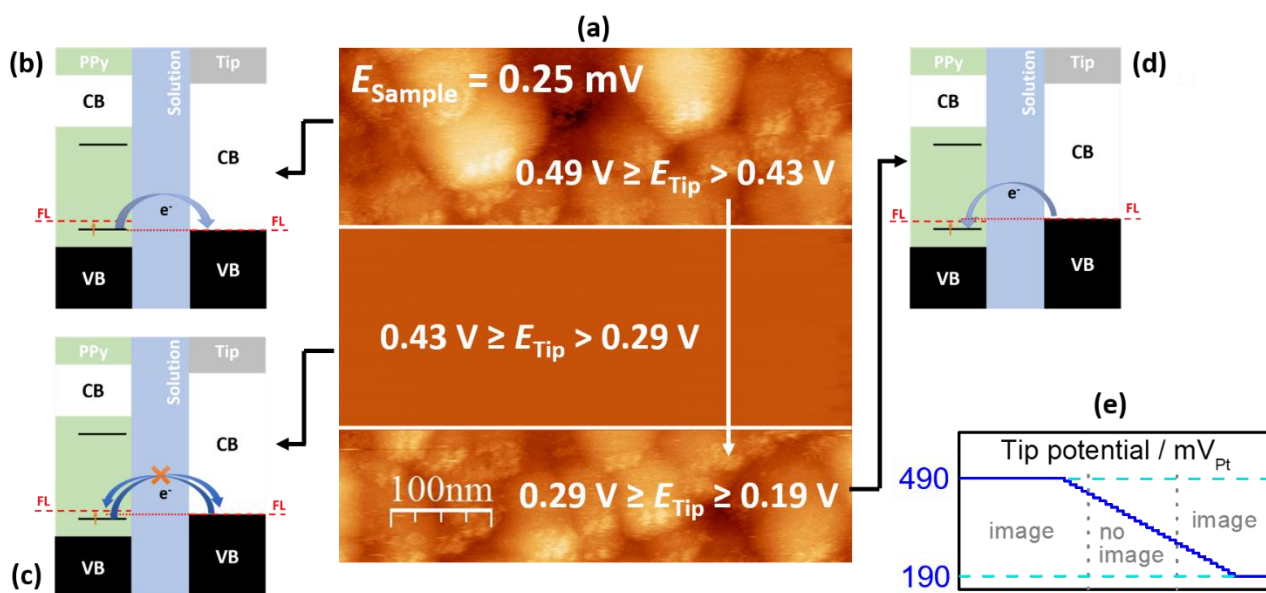
Figure 5. (a) STM image (500 x 500 nm^2) of a PPy film electrochemically grown on a Pt(111) electrode in 0.1 mol L^{-1} HClO$_4$ at E_{sample} = 0.25 V. The scan direction is from top to bottom, as indicated by the white arrow. Initially, E_{tip} = 0.49 V, and was then progressively made more negative in 0.01 V steps. The central region of the image was recorded at E_{tip} between 0.43 and 0.29 V, and the bottom section of the image at E_{tip} between 0.29 and 0.19 V; **(b)** Schematic representation of the location of the different energy levels when E_{tip} > 0.43 V, with electrons tunnelling from the intra-gap, half-filled, polaron hole state into the tip's Fermi level. The effect of band bending has been omitted for the sake of clarity and simplicity; **(c)** Schematic representation of the location of the different energy levels when E_{tip} is betwen 0.43 and 0.29 V. Tunnelling is not possible either from the tip to the sample, due to the positive tip bias, or from the sample to the tip, because there are no filled or partially filled electronic states above the tip's Fermi level; **(d)** Schematic representation of the location of the different energy levels when E_{tip} betwen 0.29 and 0.19 V. Tunnelling is now possible from the tip to the sample due to the negative tip bias and the presence of partially filled polaron levels below the tip's Fermi level. The effect of band bending has been omitted for the sake of clarity and simplicity; **(e)** Scheme illustrating the potential programme applied to the tip. I_T = 2 nA.

Our IB-EC-STS results allow us to build a quantitative energy diagram for PPy (Fig. 6). For the absolute potential scale, a value of -4.44 eV for the absolute potential of the SHE was used, as recommended by Trasatti[34], which sets the absolute potential of the RHE at pH 1 at -4.38 eV. The diagram is consistent with others reported in the literature obtained by spectroscopic methods[1,15,35].
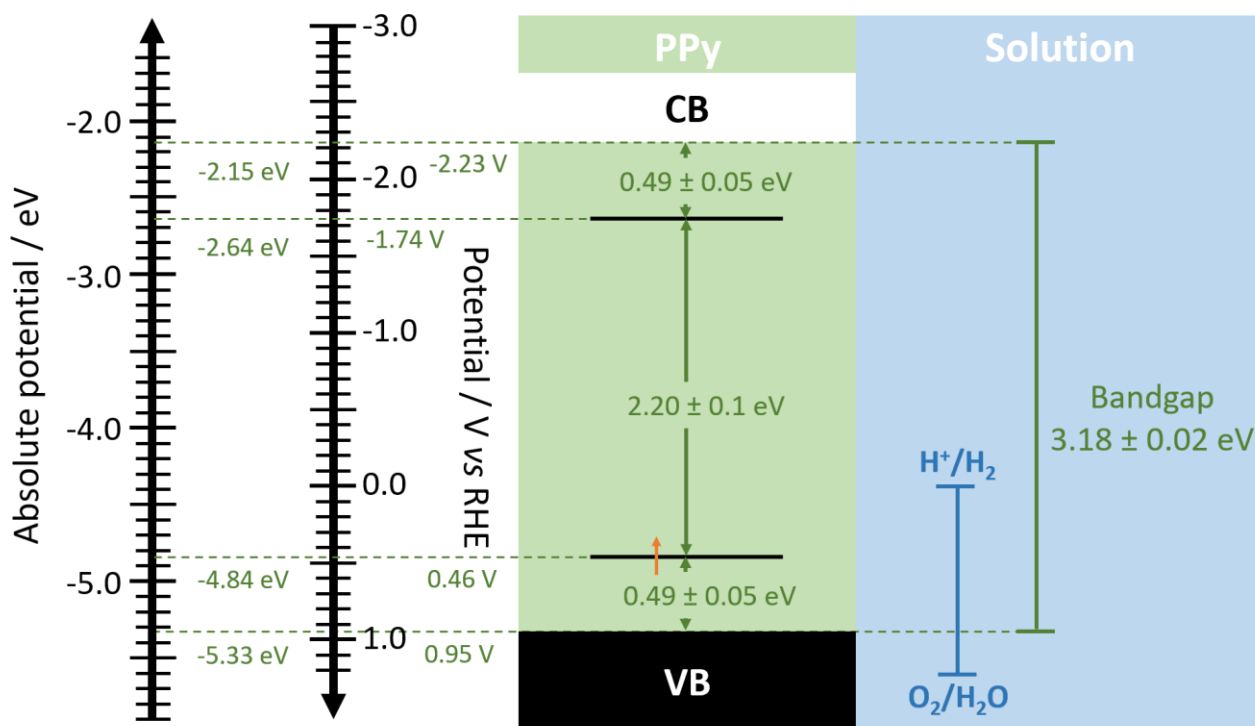
Figure 6. Band diagrams of a thin polypyrrole film on Pt as deduced from image-based electrochemical scanning tunnelling spectroscopy in 0.1 mol L^{-1} HClO$_4$. The energy levels are indicated in both the RHE and the absolute potential scales.

We would like to finish with a brief comment regarding the value of the flat-band potential as obtained from a Mott-Schottky analysis of the interfacial capacitance. The applicability and pitfalls of Mott-Schottky analysis and other methods for the determination of flat-band potentials have recently been discussed by Hankin *et al.*[36] As discussed by them, Mott Schottky analysis rests on the assumption that the capacitance of the interface is dominated by that of the semiconductor's space-charge region or that, equivalently, the potential drop across the electrolyte side of the interface is much smaller than that across the space-charge region, which might not always be the case and would limit the applicability of the Mott-Schottky equation. We would like to add here that, for materials like PPy for which the doping level is continuously increasing with increasing potential (other materials like hydrogen tungsten bronzes, whose conductivity depends on the W(V) / W(VI) ratio, could also fall in this category), the flat-band potential must also be continuously changing, which will further limit Mott-Schottky's applicability. In our particular example, we would expect the flat-band potential of undoped PPy to lie close, if not exactly at, the centre of the gap, *i.e.*, around -0.64 V vs. RHE. On the contrary, Mott-Schottky delivers a much more positive value of the apparent flat-band potential of *ca.* 0.11 V vs. RHE, only 0.35 eV higher than the polaron level. The location of the flat band

potential will be dragged down in energy as partially filled states are created some hundreds of mV above the band edge, and the apparent flat-band potential might therefore correspond instead to that of doped PPy, but the question is then what level of doping leads to this value. Alternatively, the apparent flat-band potential might indicate the onset potential of PPy oxidation (*i.e.*, of PPy doping) which would agree with the cyclic voltammogram (Fig. 1b) and the observation in Fig. 4 that tunnelling from the sample to the tip is not possible when $E_{sample} \leq 0. 1$ V and E_{tip} is more positive than E_{sample} but more negative than 0.95 V (the valence band edge). More research is probably needed to solve this question.

4. CONCLUSIONS

IB-EC-STS was demonstrated as a tool that allows to achieve a complete characterization of the band structure of a PPy film on Pt, which was consistent with the DOS spectrum obtained from electrochemical impedance spectroscopy. The advantage of IB-EC-STS over other methods is that the information regarding the electronic levels is obtained directly and does not rely on the application of a model.

REFERENCES

(1) Smyrl, W. H.; Lien, M. Electrical and Electrochemical Properties of Electronically Conducting Polymers. In *Applications of Electroactive Polymers*; Springer Netherlands: Dordrecht, 1993; pp 29–74. https://doi.org/10.1007/978-94-011-1568-1_2.

(2) Waltman, R. J.; Bargon, J.; Chemie, P.; Bonn, U.; Germany, W.; Waltman, R. J.; Bargon, J. Electrically Conducting Polymers: A Review of the Electropolymerization Reaction, of the Effects of Chemical Structure on Polymer Film Properties, and of Applications towards Technology. *Can. J. Chem.* **1986**, *64* (1), 76–95. https://doi.org/10.1139/v86-015.

(3) Yu, P. Y.; Cardona, M. Electronic Band Structures. In *Fundamentals of Semiconductors*; 2010;

pp 17–106. https://doi.org/10.1007/978-3-642-00710-1_2.

(4)   Yu, P. Y.; Cardona, M. Electrical Transport. In *Fundamentals of Semiconductors*; 2010; pp 203–241. https://doi.org/10.1007/978-3-642-00710-1_5.

(5)   Bredas, J. L.; Street, G. B. Polarons, Bipolarons, and Solitons in Conducting Polymers. *Acc. Chem. Res.* **1985**, *18* (10), 309–315. https://doi.org/10.1021/ar00118a005.

(6)   Nagaraja, A. R.; Perry, N. H.; Mason, T. O.; Tang, Y.; Grayson, M.; Paudel, T. R.; Lany, S.; Zunger, A. Band or Polaron: The Hole Conduction Mechanism in the p-Type Spinel Rh2ZnO4. *J. Am. Ceram. Soc.* **2012**, *95* (1), 269–274. https://doi.org/10.1111/j.1551-2916.2011.04771.x.

(7)   Patil, A. O.; Heeger, A. J.; Wudl, F. Optical Properties of Conducting Polymers. *Chem. Rev.* **1988**, *88* (1), 183–200. https://doi.org/10.1021/cr00083a009.

(8)   Sakellis, I.; Papathanassiou, A. N.; Grammatikakis, J. Transformation of Polarons to Bipolarons in Disordered Matter. *Appl. Phys. Lett.* **2008**, *92* (22), 222108. https://doi.org/10.1063/1.2938995.

(9)   Paasch, G.; Scheinert, S.; Petr, A.; Dunsch, L. Bipolarons or Polaron Pairs in Conducting Polymers: Equilibrium and Kinetics. *Russ. J. Electrochem.* **2006**, *42* (11), 1161–1168. https://doi.org/10.1134/S1023193506110024.

(10)   Sercheli, M. S.; Bulho, L. O. S. Polarons , Bipolarons , and Crystallization in Conducting Polymers : An ESR Study. **2000**, *631*, 631–634.

(11)   Toma, H. E. Ligação Química: Abordagem Clássica Ou Quântica? *Química Nov. na Esc.* **1997**, No. 6, 8–12.

(12)   Faez, R.; Reis, C.; FREITAS, P.; Kosima, O. Polímeros Condutores. *Química Nov. na Esc.* **2000**, No. 11, 13–18.

(13)   Wang, L.-X.; Li, X.-G.; Yang, Y.-L. Preparation, Properties and Applications of Polypyrroles. *React. Funct. Polym.* **2001**, *47* (2), 125–139. https://doi.org/10.1016/S1381-5148(00)00079-1.

(14)   Huang, Z.-B.; Yin, G.-F.; Liao, X.-M.; Gu, J.-W. Conducting Polypyrrole in Tissue Engineering Applications. *Front. Mater. Sci.* **2014**, *8* (1), 39–45. https://doi.org/10.1007/s11706-014-0238-8.

(15)   Genies, E. M.; Bidan, G.; Diaz, A. F. Spectroelectrochemical Study of Polypyrrole Films. *J. Electroanal. Chem.* **1983**, *149* (1–2), 101–113. https://doi.org/10.1016/S0022-0728(83)80561-0.

(16)   Gentz, K.; Wandelt, K. Electrochemical Scanning Tunneling Microscopy. *Chim. Int. J. Chem.* **2012**, *66* (1), 44–51. https://doi.org/10.2533/chimia.2012.44.

(17)   Zandvliet, H. J. W.; van Houselt, A. Scanning Tunneling Spectroscopy. *Annu. Rev. Anal. Chem.* **2009**, *2* (1), 37–55. https://doi.org/10.1146/annurev-anchem-060908-155213.

(18)   Yagati, A. K.; Min, J.; Choi, J.-W. Electrochemical Scanning Tunneling Microscopy (ECSTM) – From Theory to Future Applications. In *Modern Electrochemical Methods in Nano, Surface and Corrosion Science*; InTech, 2014. https://doi.org/10.5772/57236.

(19)   Wakabayashi, S.; Kato, H.; Tomitori, M.; Nishikawa, O. Scanning Tunneling Microscopy/Spectroscopy Studies of Conducting Polymer Polypyrrole. *J. Appl. Phys.* **1994**, *76* (9), 5595–5597. https://doi.org/10.1063/1.357164.

(20)   Díez-Pérez, I.; Gorostiza, P.; Sanz, F. Direct Evidence of the Electronic Conduction of the Passive Film on Iron by EC-STM. *J. Electrochem. Soc.* **2003**, *150* (7), B348. https://doi.org/10.1149/1.1580823.

(21)   García, R. Dynamic Atomic Force Microscopy Methods. *Surf. Sci. Rep.* **2002**, *47* (6–8), 197–301. https://doi.org/10.1016/S0167-5729(02)00077-8.

(22)   Yu, Z. Q.; Wang, C. M.; Du, Y.; Thevuthasan, S.; Lyubinetsky, I. Reproducible Tip Fabrication and Cleaning for UHV STM. *Ultramicroscopy* **2008**, *108* (9), 873–877. https://doi.org/10.1016/j.ultramic.2008.02.010.

(23) Zamborini, F. P.; Crooks, R. M. In-Situ Electrochemical Scanning Tunneling Microscopy (ECSTM) Study of Cyanide-Induced Corrosion of Naked and Hexadecyl Mercaptan-Passivated Au(111). *Langmuir* **1997**, *13* (2), 122–126. https://doi.org/10.1021/la960945n.

(24) Garcia-Belmonte, G.; Bisquert, J. Impedance Analysis of Galvanostatically Synthesized Polypyrrole Films. Correlation of Ionic Diffusion and Capacitance Parameters with the Electrode Morphology. *Electrochim. Acta* **2002**, *47* (26), 4263–4272. https://doi.org/10.1016/S0013-4686(02)00510-8.

(25) Bisquert, J.; Belmonte, G. G.; Santiago, F. F.; Ferriols, N. S.; Yamashita, M.; Pereira, E. C. Application of a Distributed Impedance Model in the Analysis of Conducting Polymer Films. *Electrochem. commun.* **2000**, *2* (8), 601–605. https://doi.org/10.1016/S1388-2481(00)00089-8.

(26) Otero, T. F. Biomimetic Conducting Polymers: Synthesis, Materials, Properties, Functions, and Devices. *Polym. Rev.* **2013**, *53* (3), 311–351. https://doi.org/10.1080/15583724.2013.805772.

(27) Paasch, G. Complete Electrochemical Transmission Line Model for Conducting Polymers. *Synth. Met.* **2001**, *119* (1–3), 233–234. https://doi.org/10.1016/S0379-6779(00)00865-1.

(28) Paasch, G. Transmission Line Description for Doped Conjugated Polymers with Polarons, Bipolarons and Counterions as Charged Species. *Electrochim. Acta* **2002**, *47* (13–14), 2049–2053. https://doi.org/10.1016/S0013-4686(02)00072-5.

(29) Bisquert, J.; Compte, A. Theory of the Electrochemical Impedance of Anomalous Diffusion. *J. Electroanal. Chem.* **2001**, *499* (1), 112–120. https://doi.org/10.1016/S0022-0728(00)00497-6.

(30) Gonçalves, R.; Correa, A. A. A.; Pereira, R.; Pereira, E. C. C. Investigation of the Electrochemical Aging of Poly(3-Hexiltiophene) Using Impedance Spectroscopy. *Electrochim. Acta* **2016**, *190*, 329–336. https://doi.org/10.1016/j.electacta.2015.12.198.

(31)   Correa, A. A.; Gonçalves, R.; Pereira, R.; Pereira, E. C. The Electropolymerization of Several Poly(3-Methylthiophene) Films in the Same Used Solution and Its Consequence in Their Properties. *J. Appl. Polym. Sci.* **2017**, *134* (2). https://doi.org/10.1002/app.44368.

(32)   Gmucová, K.; Nádaždy, V.; Schauer, F.; Kaiser, M.; Majková, E. Electrochemical Spectroscopic Methods for the Fine Band Gap Electronic Structure Mapping in Organic Semiconductors. *J. Phys. Chem. C* **2015**, *119* (28), 15926–15934. https://doi.org/10.1021/acs.jpcc.5b04378.

(33)   Nádaždy, V.; Schauer, F.; Gmucová, K. Energy Resolved Electrochemical Impedance Spectroscopy for Electronic Structure Mapping in Organic Semiconductors. *Appl. Phys. Lett.* **2014**, *105* (14), 142109. https://doi.org/10.1063/1.4898068.

(34)   Trasatti, S. The Absolute Electrode Potential: An Explanatory Note. *J. Electroanal. Chem. Interfacial Electrochem.* **1986**, *209* (2), 417–428. https://doi.org/10.1016/0022-0728(86)80570-8.

(35)   Santos, M. J. L. J. L.; Brolo, A. G. G.; Girotto, E. M. M. Study of Polaron and Bipolaron States in Polypyrrole by in Situ Raman Spectroelectrochemistry. *Electrochim. Acta* **2007**, *52* (20), 6141–6145. https://doi.org/10.1016/j.electacta.2007.03.070.

(36)   Hankin, A.; Bedoya-Lora, F. E.; Alexander, J. C.; Regoutz, A.; Kelsall, G. H. Flat Band Potential Determination: Avoiding the Pitfalls. *J. Mater. Chem. A* **2019**, *7* (45), 26162–26176. https://doi.org/10.1039/C9TA09569A.